AGU PUBLICATIONS

Global Biogeochemical Cycles

RESEARCH ARTICLE
10.1002/2016GB005392

Convergent approaches to determine an ecosystem's transpiration fraction

M. Berkelhammer[1], D. C. Noone[2], T. E. Wong[3,4], S. P. Burns[5,6], J. F. Knowles[5,7], A. Kaushik[4,8], P. D. Blanken[5], and M. W. Williams[5,7]

[1]Department of Earth and Environmental Sciences, University of Illinois at Chicago, Chicago, Illinois, USA, [2]College of Earth, Ocean and Atmospheric Sciences, Oregon State University, Corvallis, Oregon, USA, [3]Department of Applied Mathematics, University of Colorado Boulder, Boulder, Colorado, USA, [4]Cooperative Institute for Research in Environmental Sciences, University of Colorado Boulder, Boulder, Colorado, USA, [5]Department of Geography, University of Colorado Boulder, Boulder, Colorado, USA, [6]National Center for Atmospheric Research, Boulder, Colorado, USA, [7]Institute of Arctic and Alpine Research, University of Colorado Boulder, Boulder, Colorado, USA, [8]Department of Atmospheric and Oceanic Sciences, University of Colorado Boulder, Boulder, Colorado, USA

Key Points:
- Two approaches to derive plot-scale T/ET produce consistent results at sites with a factor of 3 difference in LAI
- Average T/ET values were found to be 0.6 and 0.5 for the sites, which are consistent with expected controls of LAI on T/ET
- T/ET was invariant on monthly to interannual timescales implying an inherent stability in how these ecosystems distributed latent heat

Correspondence to:
M. Berkelhammer,
berkelha@uic.edu

Citation:
Berkelhammer, M., D. C. Noone, T. E. Wong, S. P. Burns, J. F. Knowles, A. Kaushik, P. D. Blanken, and M. W. Williams (2016), Convergent approaches to determine an ecosystem's transpiration fraction, *Global Biogeochem. Cycles*, *30*, 933–951, doi:10.1002/2016GB005392.

Received 15 FEB 2016
Accepted 29 MAY 2016
Accepted article online 6 JUN 2016
Published online 30 JUN 2016
Corrected 31 AUG 2018

This article was corrected on 31 AUG 2018. See the end of the full text for details.

Abstract The transpiration (T) fraction of total terrestrial evapotranspiration (ET), T/ET, can vary across ecosystems between 20–95% with a global average of ~60%. The wide range may either reflect true heterogeneity between ecosystems and/or uncertainties in the techniques used to derive this property. Here we compared independent approaches to estimate T/ET at two needleleaf forested sites with a factor of 3 difference in leaf area index (LAI). The first method utilized water vapor isotope profiles and the second derived transpiration through its functional relationship with gross primary production. We found strong agreement between T/ET values from these two independent approaches although we noted a discrepancy at low vapor pressure deficits (VPD). We hypothesize that this divergence arises because stomatal conductance is independent of humidity at low VPD. Overall, we document significant synoptic-scale T/ET variability but minimal growing season-scale variability. This result indicates a high sensitivity of T/ET to passing weather but convergence toward a stable mean state, which is set by LAI. While changes in T/ET could emerge from a myriad of processes, including aboveground (LAI) or belowground (rooting depth) changes, there was only minimal interannual variability and no secular trend in our analysis of T/ET from the 15 year eddy covariance time series at Niwot Ridge. If the lack of trend observed here is apparent elsewhere, it suggests that the processes controlling the T and E fluxes are coupled in a way to maintain a stable ratio.

1. Introduction

Transpiration is the largest component of the terrestrial latent heat budget with estimates suggesting that it accounts for somewhere between 50 and 90% of the annual global land surface water flux [*Good et al.*, 2015; *Jasechko et al.*, 2013; *Schlesinger and Jasechko*, 2014; *Wang et al.*, 2014]. Transpiration impacts numerous components of the global hydrological cycle including cloud formation, precipitation processes, groundwater dynamics, streamflow, and atmospheric humidity [e.g., *Worden et al.*, 2007; *Farley et al.*, 2005; *Dunn and Mackay*, 1995]. Therefore, shifts in its magnitude either through changes in climate, land use, atmospheric chemistry, or ecosystem structure could have large global impacts. According to *Frank et al.* [2015], there has been a recent global increase in transpiration implying that its sensitivity to global change is already perceptible. However, the processes controlling an ecosystem's transpiration rate at hourly to intraseasonal timescales are not well known because the most direct approaches to estimate this flux (i.e., sap flow and leaf-level gas exchange measurements) are difficult to scale up to the ecosystem or regional level. The alternative to a direct estimate of transpiration (T) is to partition the ecosystem latent heat flux (evapotranspiration (ET)), which can be well constrained using eddy covariance [*Law et al.*, 2002], into biotic (T) and abiotic (i.e., leaf interception and soil evaporation, E) components [*Kool et al.*, 2014]. Hereafter, we refer to the transpiration component of the total latent heat flux as T/ET following a number of recent studies [*Good et al.*, 2015; *Wang et al.*, 2014; *Jasechko et al.*, 2013].

Both T and E are controlled to a first order by soil moisture availability, atmospheric humidity, and turbulent characteristics. If we were to consider a simple case where the leaf area index (LAI) was 1.0 and plants were shallow rooted, T and E would both utilize the same water source and have the same surface area from

which to evaporate. In this case, the two would be closely coupled except under periods of low humidity when stomatal conductance would decrease T but E would remain high. It could be anticipated that E would consistently exceed T, leading to T/ET values below 0.5. If LAI were to exceed 1.0, but plants are still shallow rooted, the surface area from which T is generated has now increased, but the effect of decreased humidity on stomatal conductance would remain. There would be an increase in overall T/ET with a magnitude set by LAI and the stomatal response to humidity. In this scenario, if rooting depth were to increase, T and E would be drawn from distinct water sources. Under periods of water stress, E would be reduced as surface waters decreased, but T could remain stable because of plant access to water at depth. T would consistently exceed E (i.e., $T/ET \geq 0.5$), which is the common state across ecosystems [*Schlesinger and Jasechko*, 2014]. The complex interplay between climate, biomass allocation (root depth and LAI), and soil hydrology could act to couple T and E and maintain stable T/ET values or decouple T and E leading to a shift in T/ET. However, testing hypotheses on the controls of T/ET have consistently been hindered by a lack of approaches to directly estimate this property in the field.

One approach toward deriving T/ET is to isolate the shared, or stomatal-driven, component of an ecosystem's carbon and water fluxes derived using eddy covariance [*Scanlon and Kustas*, 2010; *Reichstein et al.*, 2012]. There is a close correlation between T and gross primary production (GPP) rates; thus, if one is known, the other can be inferred [*Law et al.*, 2002; *Ball et al.*, 1987; *Wong et al.*, 1978]. However, this requires partitioning of the total carbon flux into respiration and GPP [*Reichstein et al.*, 2005; *Falge et al.*, 2001; *Kuglitsch et al.*, 2008; *Beer et al.*, 2009; *Law et al.*, 2002] and an assumption that the slope between the two (i.e., water use efficiency) is stable [*Scanlon and Kustas*, 2010]. Studies on the coupling between the terrestrial carbon and water cycles have used turbulent nighttime carbon fluxes to derive a temperature model for soil respiration, which is applied to partitioning the carbon flux. Transpiration is then assumed to be linearly proportional to ET [e.g., *Beer et al.*, 2009; *Keenan et al.*, 2013]. While these efforts aim to isolate the ecosystem control on water and carbon fluxes, neither directly compare transpiration with modeled GPP. While efforts to take advantage of the correlation between carbon and water fluxes to derive T/ET have been pursued [e.g., *Kool et al.*, 2014; *Zhou et al.*, 2016], this approach remains fairly uncommon.

An alternative to deriving T/ET from carbon and water fluxes is to utilize stable water isotope ratios ($^{18}O/^{16}O$ and $^{2}H/^{1}H$). This approach has been adapted for ET partitioning for many years based on an understanding that because E is fractionated and T is not, the two fluxes have distinct isotopic signatures [*Yepez et al.*, 2003; *Wang and Yakir*, 2000; *Williams et al.*, 2004; *Moreira et al.*, 1997; *Wershaw et al.*, 1966]. Thus, the isotopic composition of the water vapor in the canopy provides an instantaneous perspective on the relative contributions of E and T [*Yakir and Sternberg*, 2000], and residual water pools in an ecosystem (e.g., streamflow or soil water) are thought to be sensitive integrators of whether water was removed via E or T [*Jasechko et al.*, 2013]. The isotope partitioning approach has origins that are decades old [*Zimmermann et al.*, 1966; *Allison and Barnes*, 1983], but its regular application has been limited both by the technical challenges associated with measurements of water vapor isotopes and the challenge of accurately modeling the isotopic ratios of the E and T fluxes [*Good et al.*, 2012; *Seibt et al.*, 2006; *Lee et al.*, 2009]. Recently, however, the approach has become increasingly widespread due both to the proliferation of in situ laser-based isotope spectroscopy and larger available databases of stable water isotopes [*Sutanto et al.*, 2014; *Jasechko et al.*, 2013; *Good et al.*, 2014; *Wang et al.*, 2014, 2010].

Global analyses of T/ET have been undertaken using stable isotopes of large lakes [*Jasechko et al.*, 2013], remote sensing of water isotope ratios [*Good et al.*, 2015], and metaanalyses taking advantage of a diversity of approaches [*Schlesinger and Jasechko*, 2014; *Wang et al.*, 2014]. With the exception of *Jasechko et al.* [2013], who estimated a global T/ET value of ~0.90, the other studies converge on T/ET values of ~0.60–0.65. *Schlesinger and Jasechko* [2014] suggest this wide range of global T/ET estimates (~0.25–0.3), in part, reflects differences in how previous studies have treated the amount of precipitation that is intercepted by leaves and evaporated back to the atmosphere without reaching the soil. *Good et al.* [2015] find that interception accounts for 27% of the terrestrial ET budget, leading to an estimate of global T/ET of ~0.6, which is on the lower end of previous estimates. This value contrasts the findings of *Jasechko et al.* [2013], who estimate interception rates to be 7% of ET, which yields a global T/ET estimate of ~0.9.

These existing studies neither address the dynamics that drive temporal variability of T/ET nor whether the different techniques agree across diverse landscapes. More specifically, the range of spatiotemporal scales that the different methods are sensitive to limit the degree to which the potential for convergence between

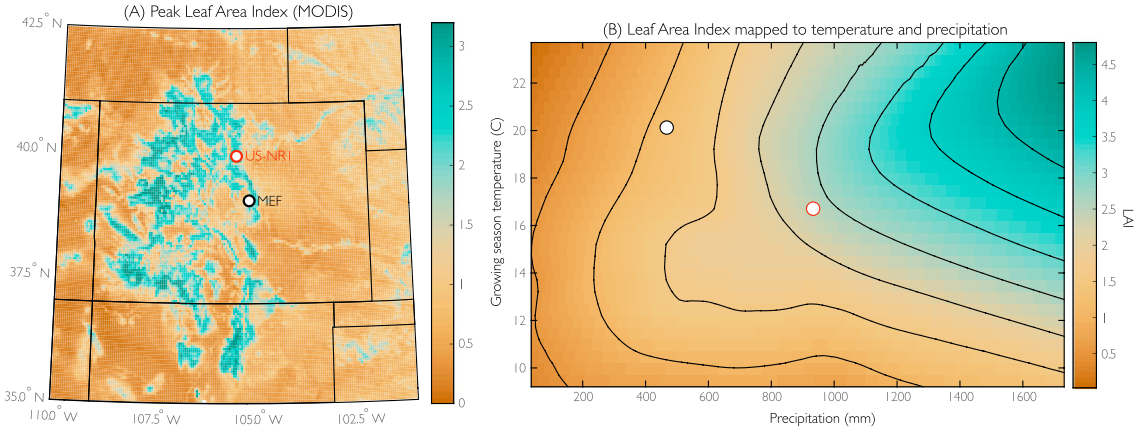

Figure 1. (a) Map of average maximum annual leaf area index from MODIS [*Xiao et al.*, 2014] with US-NR1 (red) and MEF (black) sites. As discussed in section 4, there is a low bias in the MODIS LAI estimates for US-NR1. (b) Surface fit between average LAI, July maximum air temperature [*Oyler et al.*, 2015] and annual precipitation for all the SNOTEL sites [e.g., *Serreze et al.*, 1999] in the Rocky Mountains. Contours are approximately 0.5 m^2 m^{-2} increments. The approximate conditions at US-NR1 (red) and MEF (black) sites are plotted onto this surface.

approaches can be evaluated. For example, *Jasechko et al.* [2013] rely on lakes which integrate watersheds with residence times of years to decades, whereas sap flow sensors or flux chambers record the instantaneous behavior at subplot scales. Therefore, the response of T/ET dynamics to hydrological events such as drought or floods (synoptic to seasonal timescales) or to secular changes such as the stomatal response to rising carbon dioxide (CO_2), "greening" or changes in snowpack dynamics associated with warming are unknown. Understanding the response of T/ET to various forcing mechanisms is critical for assessing how hydrological partitioning is represented in land surface models. Consequently, the current lack of observational constraints on T/ET at the subregional scale inhibits quantitative assessment of how models capture dynamic elements of this first-order ecohydrological property.

To better evaluate the similarities between two widely applicable approaches to derive T/ET, we evaluated its variability at two needleleaf forested sites (Niwot Ridge AmeriFlux tower and Manitou Experimental Forest) with distinct leaf area indices (LAI; 4.2 m^2 m^{-2} and 1.2 m^2 m^{-2}, respectively). One approach utilized standard eddy covariance products and is based on the correlation between carbon and water fluxes [*Zhou et al.*, 2016] and the other approach used profiles of the stable isotope ratio of water vapor [*Yakir and Sternberg*, 2000]. We set out to (1) compare the relative strengths of these two independent approaches to quantify T/ET, and then we used this information to (2) gain a better understanding of the controls and temporal scales of T/ET variability between sites with a large difference in LAI. The results show an agreement between the approaches at both sites with a difference in the mean T/ET between sites that compares well with expected controls of LAI on T/ET [*Wang et al.*, 2014].

2. Methods

2.1. Locations

The analyses presented here were conducted at two sites: the Niwot Ridge AmeriFlux tower (40.03°N, −105.55°W) and the Manitou Experimental Forest (39.08°N, −105.07°W) (Figure 1). Niwot Ridge (US-NR1) is ~140 km north of Manitou Experimental Forest (MEF) and is ~500 m higher (3023 m as opposed to 2503 m for MEF). Despite their relatively close proximity, the two forests experience distinct climates owing to the complex topography in the region. US-NR1 receives approximately double the annual precipitation as MEF (884 mm versus 430 mm), has a colder average air temperatures (e.g., July 14°C for US-NR1 and 19°C for MEF) and a more sustained winter and spring snowpack [*Ortega et al.*, 2014; *Burns et al.*, 2015]. These differences in climate and hydrology between sites and different land use histories (MEF was heavily logged in the 1920s [*Johnson*, 1956]) produce distinct canopy structures. Specifically, US-NR1 has a relatively denser canopy (LAI 4.2 m^2 m^{-2}) compared to the open canopy at MEF (LAI 1.2 m^2 m^{-2}) (Figure 1).

2.2. Niwot Ridge

US-NR1 has operated as part of the AmeriFlux network continuously since 1998 [*Burns et al.*, 2015; *Monson et al.*, 2002; *Knowles et al.*, 2015a]. It includes a 26 m walk-up tower within a subalpine mixed coniferous

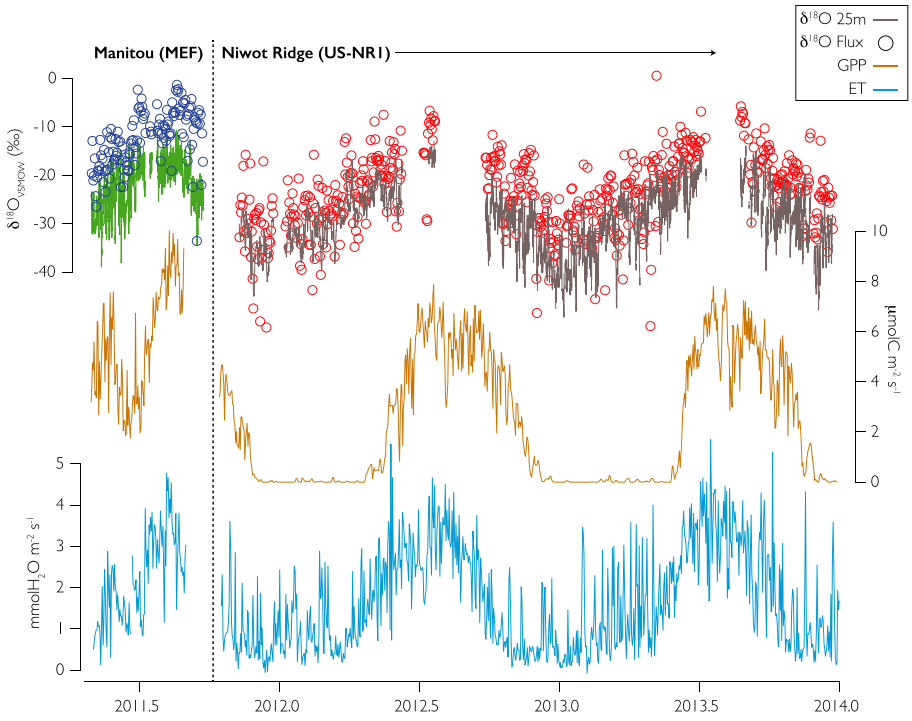

Figure 2. (top) Time series of the hourly mean $\delta^{18}O$ (lines) and $\delta^{18}O_{ET}$ (dots) for the Niwot Ridge and Manitou Experimental Forest sites. Two long data gaps occur during both the 2012 and 2013 summers due to overheating in the shed and a failed vacuum pump. (middle) Time series of diel (6:00–18:00) mean GPP for the Manitou and Niwot Ridge sites calculated using the flux partitioning method of *Reichstein et al.* [2005]. (bottom) Time series of diel mean ET flux for both sites using eddy covariance.

forest with a canopy height of ~11 m. The tower includes an eddy covariance system for assessing CO_2, H_2O, and sensible heat fluxes using a combination of a sonic anemometer and fast response temperature sensors and gas analyzers. Data from the eddy covariance system as well as other measurements made from the tower are available through the AmeriFlux data portal (ameriflux.ornl.gov) and the tower website (urquell.colorado.edu/data_ameriflux/data_30min/). The tower footprint is dominated by subalpine fir (*Abies lasiocarpa*), Engelmann spruce (*Picea engelmannii*), lodgepole pine (*Pinus contorta*), and minimal understory vegetation. More details on site characteristics including instrumentation, climatology, hydrology, plant water utilization, and carbon fluxes are discussed in a number of previous publications [e.g., *Monson et al.*, 2002; *Blanken et al.*, 2009; *Turnipseed et al.*, 2002; *Hu et al.*, 2010; *Burns et al.*, 2015; *Knowles et al.*, 2015b]. Following *Bowling et al.* [2014], the filtered eddy covariance data were used to derive a 30 min GPP flux with the *Reichstein method* [*Falge et al.*, 2001; *Reichstein et al.*, 2005]. We utilized "version2011.04.20" of the flux and climate data [*Burns et al.*, 2015].

In addition to the aforementioned data, this study also used the stable isotopic ratios of water vapor ($^{18}O/^{16}O$ and $^{2}H/^{1}H$) measured from a Picarro l2120-i analyzer that was installed in a small shed at the base of the tower during the fall of 2011. The instrument was set up to retrieve profiles of the stable isotopic ratio of water vapor from eight heights within and above the canopy using cavity ringdown spectrometry [*Gupta et al.*, 2009]. Five of the sampling inlets were installed directly on the tower at heights of approximately 5, 10, 15, 20, and 25 m, and three of the inlets were installed on a nearby tree at heights of approximately 1, 2, and 3 m. The air samples entered 9.652 cm (0.25 inch) OD copper tubing through a heated orifice at the inlet to minimize condensation within the line. All sample lines were ~30 m long, such that the pressure drop in the lines was similar and therefore minimized abrupt pressure fluctuations during manifold valve switching. Air was moved through the lines at a rate of ~6–8 L min^{-1} using a regenerative blower.

The sample lines were attached to a solenoid manifold, which went through an automated sequence of analyzing each inlet for 10 min. The first 5 min of data following the switch between sampling inlets were excluded from subsequent analysis to minimize memory effects associated with previous air samples not

entirely flushed from the parts of the system's plumbing that were common to all air samples. The system was periodically leak checked by swabbing ethanol onto all potential leak sources (e.g., compression unions and solenoids). The alcohol interferes with the instrument spectroscopy and minute quantities entering the optical cavity produce strong evidence of leaks. The system was generally calibrated every 3–6 h with the Picarro Inc. *Standards Delivery Module* (Model Number: A0101), which used a syringe pump to introduce one of two reference waters into a vaporizer kept at 140°C. The reference water vapor was mixed with varying amounts of dry air (created by pulling ambient air through a desiccant) to produce air with different humidities but the same isotopic ratio. The calibration stream entered the isotopic analyzer through a three-way solenoid valve that switched between air samples from the tower and from the two reference waters. Repeated measurements of reference waters over the course of 3 years of measurements indicated a precision on 5 min averaged values for $\delta^{18}O$ of $\leq$0.6 ‰. The calibration system experienced many down periods during this experiment owing either to periodic clogging of the syringes/flow lines and a failed air pump (noted by data gaps in Figure 2).

Temperature and humidity dependence of the isotopic data were estimated by measuring the reference waters across a range of humidities and temperatures; the latter of which was generated through seasonal and diurnal changes in the instrument shed's temperature. The concentration dependence of the isotopic measurement (i.e., "humidity effect"), which is well documented [e.g., *Schmidt et al.*, 2010; *Johnson et al.*, 2011], is instrument specific but stable over time [*Bailey et al.*, 2015]. Therefore, calibration data over the course of the multiple years of analysis were combined to generate a universal humidity correction, which was applied to all the data (Figure 3a). Temperature effects were negligible across the ~15°C that the instrument varied (Figure 3b). During a few brief periods when shed ventilation was disrupted, the temperature conditions exceeded this threshold, and these data were excluded from the analysis. Although the temperature and humidity effects can be severe, they are negligible in the context of this study because the focus of the analysis is during the spring (for reasons discussed below), when the instrument was operating at optimal conditions. The experimental setup, quality control, and data processing are virtually identical to those presented in *Berkelhammer et al.* [2013]. While the analysis presented hereafter focuses on $\delta^{18}O$ and only discusses in detail data from the spring and during the daytime hours (6:00–18:00 local time and GPP > 0), all data from the uppermost inlet are publicly available as part of the AmeriFlux data products for this site (urquell.colorado.edu/data_ameriflux/data_30min/) and data from the other heights are available upon request.

2.2.1. Manitou Experimental Forest

The MEF site is in an open-canopy forest populated almost exclusively with *Pinus ponderosa*. The measurements discussed here were made during the 2011 growing season when the site was heavily instrumented as part of the bio-hydro-atmosphere Interactions of energy, aerosols, carbon, H_2O, organics, and nitrogen-Rocky Mountain Biogenic Aerosol Study project [*Ortega et al.*, 2014]. From the measurements available during this period, we utilized VPD, air temperature, soil moisture, soil temperature, and a suite of standard eddy covariance products (e.g., friction velocity, CO_2 flux and H_2O flux). GPP for the site was derived following the same flux partitioning technique utilized at US-NR1 [i.e., *Falge et al.*, 2001; *Reichstein et al.*, 2005]. Isotopic measurements were made from May to September 2011 using a different Picarro l2120-i analyzer installed in a temperature-controlled shed at the base of the 27.1 m tower. Calibration and processing of the isotopic data were reported by *Berkelhammer et al.* [2013]. Briefly, six inlets were installed at 1.5, 5.0, 8.5, 12.0, 17.7, and 25.1 m, and each inlet was sampled for 5 min in sequence. The methodology is similar to that utilized for the US-NR1 site and for this study was binned onto the same 1 h time step to minimize the effects of resolution when comparing results between sites. *Ortega et al.* [2014] should be referred to for additional details on site characteristics and instrumentation.

2.3. Partitioning of ET

2.3.1. Optimal Partitioning Approach

For each of the sites, we partitioned ET using two independent approaches. The first approach, which hereafter is referred to as the "optimal approach," utilized standard eddy covariance products available from both sites. This approach has two inherent assumptions: (1) stomatal dynamics minimize the amount of transpiration for a given rate of GPP, which has a theoretical basis in established photosynthetic and humidity controls on stomatal conductance [*Ball et al.*, 1987] and (2) there are periodic 30 min windows across the spectrum of GPP measurements when the transpiration fraction (T/ET) approaches 1 (i.e., nearly all the latent heat flux is from transpiration). Therefore, within a narrow GPP range, any ET that is greater than the minima within that

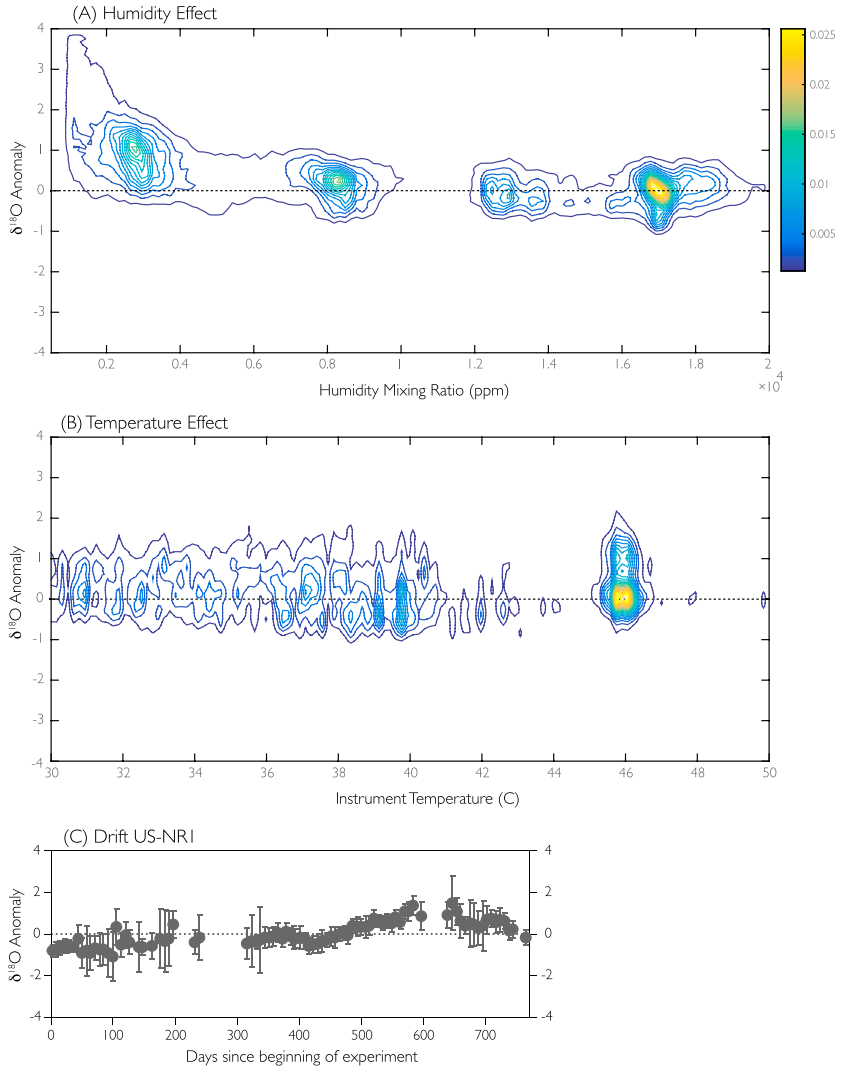

Figure 3. (a) The effect of water vapor mixing ratio on the $\delta^{18}O$ of the vapor for the US-NR1 site. The contours and color bar show the density of measurements at different humidities over the entire period the instrument has operated at the site. A fit to the data is used to generate the humidity correction. The effect is not measurable during the spring and summer seasons. (b) Same as Figure 3a but showing how the isotopic ratios vary as instrument temperature changes. To minimize the humidity effect, only data taken when the humidity is high are used to assess the temperature effect. (c) Reference waters measured over a 2 year period with error bars capturing the standard deviation of the reference water injection. The data discussed in the text have been corrected to adjust both for the humidity effect (Figure 3a) and drift (Figure 3c). In all panels, the *y* axis is the anomaly from the known isotopic ratio of the reference.

window must be associated with a flux other than transpiration such as evaporation from soil or leaf surfaces. It is important to note that in this method interception and evaporation are not distinguished [*Good et al.*, 2015] but collectively represent the abiotic component of the latent heat flux.

To derive T/ET through this approach, ET is plotted against GPP × $VPD^{0.5}$, which linearizes the relationship between GPP and ET by normalizing the fluxes to VPD [*Beer et al.*, 2009; *Zhou et al.*, 2014]. A curve is then fit to the minimum ET found at each 0.1 normalized GPP bin (Figure 4). The size of the bin is arbitrary but reflects a trade-off between sufficient data within each bin to minimize the effect of outlying values, but not such a large bin as to include dissimilar data together. Because of errors in the flux estimates that arise from a combination of processing the eddy covariance data, noise/bias in the gas analyzers and uncertainties in the respiration model used to estimate GPP from net ecosystem CO_2 exchange, the singular ET minimum within a bin is often an outlier. In order to generate a well-conditioned function, we defined the minimum as the 5th percentile of ET for each GPP bin. The choice of the correct percentile cutoff to define the minimum ET is

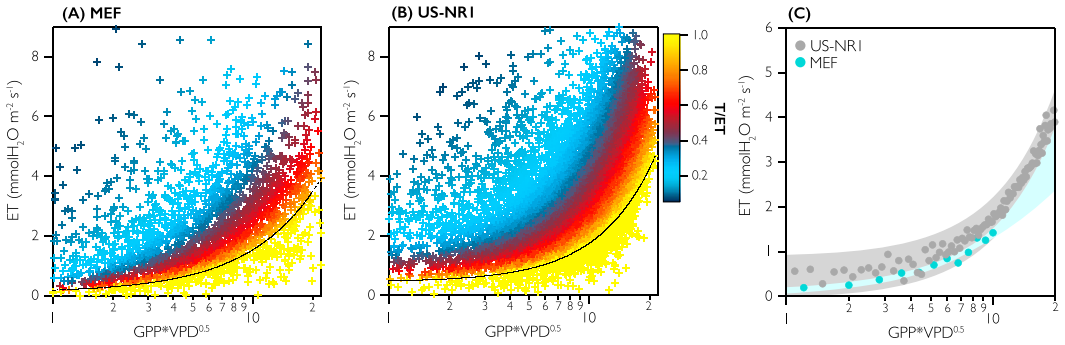

Figure 4. ET plotted against GPP after normalization of GPP following *Zhou et al.* [2014] has been applied. The black line is the fit between the 5th percentile of ET for each 0.1 GPP × $VPD^{0.5}$ bin, which represents the cutoff for which all values at or below are assumed to have a T/ET equal to 1. The coloring of the crosses is the T/ET which was derived for each point using equation (1). Data are plotted on a log scale to highlight the lower end of the GPP data. The data used to generate the black line in Figures 4a and 4b are shown in Figure 4c as colored dots. The fit to the dots with a second-order power law and the 95% confidence interval to the fit is shown by the shading. The data were poorly conditioned for MEF at high GPP values due to a scarcity of data, and the fit was extrapolated to the full range of the US-NR1 data using the regression equation.

unknown and may vary between sites depending on plant functional types, LAI, or in the presence of biases in one or both of the gas analyzers used. The cutoff value can be considered an error term because if the ET and GPP measurements were perfect, the value should be 0 [*Zhou et al.*, 2016]. A sensitivity analysis for this term was done by varying the percentile cutoff between 0 and 10% (Figure 5). The results indicate that the choice for this value will influence the mean T/ET by ±0.05 but will not affect the observation of a significant difference between T/ET for the two sites (Figures 5 and 6). Hereafter, any values falling on (or below) the line between GPP and the 5th percentile of the binned ET are considered to have a T/ET value of 1 and for all additional points T/ET is the ratio between the observed and minimum ET:

$$T/ET_{optimal} = \frac{\min_{GPP} \|ET\|}{ET_{flux}} \quad (1)$$

As with the isotope approach, only daytime values were used (6:00–18:00 local time and GPP > 0) and when friction velocity (u_*) exceeded 0.15 m s^{-1}.

2.3.2. Isotope Partitioning Approach

2.3.2.1. Niwot Ridge

The isotope partitioning approaches utilized a two end-member (E and T) mixing model, where *R* is the ratio of the heavy to light isotope (in this case, $^{18}O/^{16}O$) [*Yakir and Sternberg*, 2000]:

$$T/ET_{isotope} = \frac{R_{ET} - R_E}{R_T - R_E} \quad (2)$$

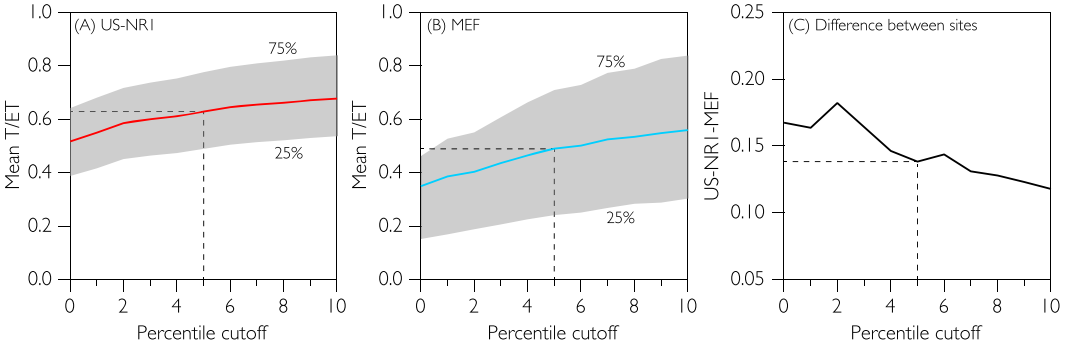

Figure 5. Sensitivity analysis showing how the derived T/ET values using the optimal approach (Figure 4) are influenced by the choice of the cutoff ET percentile (i.e., the point at which T/ET is assumed equal to 1) for (a) US-NR1 and (b) MEF. (C) The difference between the sites as a function of the cutoff percentage. The dotted line shows the cutoff percentage (5%) adopted for the analyses discussed in the text.

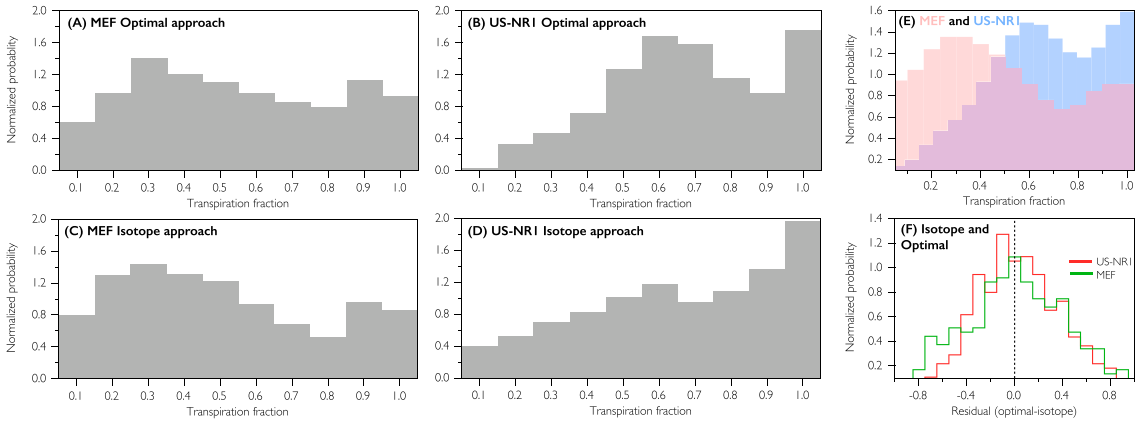

Figure 6. (a and c) Normalized distributions of T/ET for MEF using the optimal (Figure 6a) and isotope (Figure 6c) approaches. (b and d) Normalized distributions of T/ET for US-NR1 using the optimal (Figure 6b) and isotope (Figure 6d) approaches. (e) Normalized distribution of T/ET for MEF and US-NR1 using all data (i.e., both isotope and optimal) for both sites. (f) Distribution of the difference between isotope and optimal approaches for both sites.

To solve this equation, estimates of the isotopic ratio of the ET, E, and T fluxes are needed. At both sites, the former is solved for using a modified "Keeling plot" approach as described by *Noone et al.* [2013]. The data from each height were binned on hourly time steps to generate vertical profiles, and the three uppermost inlets (above the canopy) were used to estimate the isotopic ratio of the canopy's latent heat flux ($\delta^{18}O_{ET}$). Flux estimates were calculated only when the correlation between the inverse of the mixing ratio of water and the isotopic ratio of the water exceeded 0.8 and u_* exceeded 0.15 m s^{-1}. The approach followed that of *Miller and Tans* [2003] but applied to vertical profiles following *Noone et al.* [2013]. The solution was derived using equation (3) where q is the mixing ratio of water, δ is the isotopic ratio reported relative to VSMOW [*Coplen*, 1988], and *background* is the isotopic ratio of the water vapor measured at the 25 m inlet. The flux was then solved for as the slope of the regression line fit to $q \cdot \delta^{18}O$ against q:

$$q \cdot \delta^{18}O = q \cdot \delta^{18}O_{ET} - \left[q_{background} \cdot \left(\delta^{18}O_{ET} - \delta^{18}O_{background}\right)\right] \quad (3)$$

The isotopic ratio of the E and T fluxes were not directly obtained from the measurements and were derived by modeling the E and T fluxes (section 2.3.2.2).

2.3.2.2. E and T Fluxes Estimates at US-NR1

E and T fluxes were estimated using the following equation from *Craig and Gordon* [1965] where h is the relative humidity of the air with respect to the surface temperature, α_k is the canopy kinetic fractionation factor, α^* is the temperature-dependent fractionation factor during phase change, R_{source} is either the water in the leaf or the soil/snowpack and *canopy* is the isotopic ratio of the vapor measured at 8 m:

$$R_{E\,or\,T} = \frac{1}{\alpha_k \alpha^* (1-h)} \cdot R_{source} - \alpha^* h \cdot R_{canopy} \quad (4)$$

The temperature-dependent fractionation factor was estimated following *Horita and Wesolowski* [1994], where the temperature is taken as the 2 m air temperature for E and the 8 m air temperature for T. We used these different temperatures to capture periods when the temperature near the surface is not equivalent to that in the canopy. The kinetic fractionation factor (α_k) for evaporation and transpiration fluxes are related to one another through the resistance between the canopy and atmosphere but are distinct in that the former is sensitive to resistances at the soil surface and between the soil surface and canopy, whereas the latter is sensitive to resistances at the stomata and leaf boundary [*Riley et al.*, 2002]. Here we followed the approach of *Lee et al.* [2009] to estimate all the relevant resistance terms, and we considered the transpiration and evaporation kinetic fractionation factors as distinct. All relevant equations are included in Appendix 1. We ignored the kinetic effects associated with the interception stream, which in our analysis of T/ET was considered part of the evaporation component of the ET budget. This maintained consistency with the optimal approach, which had no basis for separating interception from soil evaporation. The interception stream would experience a

smaller kinetic fractionation effect than the soil as it bypasses resistances at the soil interface and between the soil surface and canopy. The potential biases associated with this simplification are discussed in section 4.

Following *Dubbert et al.* [2014] and *Seibt et al.* [2006], we estimated the isotopic ratio of the leaf water by calculating its instantaneous deviation from the steady state condition (i.e., when the transpiration stream is isotopically equivalent to the xylem water) [*Barbour et al.*, 2004]. Equation (5) describes the isotopic ratio of the leaf water at steady state (R_{leafSS}); therefore, equation (4) may be rewritten as follows:

$$R_{leafSS} = \alpha_K \cdot \alpha_T \cdot (1 - h) \cdot R_{source} + \alpha_T \cdot h \cdot R_{canopy} \quad (5)$$

Equation (6) then estimates the non-steady state leaf water isotopic ratio ($R_{leafNSS}$) using further information on stomatal conductance (*Gs*) and the leaf water volume (*Vol*). The former is calculated through inversion of the Penman-Monteith equations [*Monteith*, 1981], and the latter is taken from *Seibt et al.* [2006]:

$$R_{leafNSS}(t) = R_{leafSS}(t) + [R_{leafSS}(t) - R_{leafNSS}(t-1)] \cdot e^{-(1-\alpha_K)\cdot(1-\alpha_T)\cdot\frac{timestep}{\frac{Vol}{G_s}}}; \quad (6)$$

In order to solve equation (6), the stable isotopic ratio of the leaf water must be initialized (i.e., at time = *t*-1). To address this, we adopt the convention that there is an instantaneous moment every afternoon when the leaf reaches steady state at which point the system is reinitialized [*Seibt et al.*, 2006]. The justification for this is that when the transpiration rate is high, the turnover of leaf water compared to the volume of leaf water leads to the system reaching steady state. However, the actual moment when steady state is reached is unknown and presumably varies between days. Thus, a Monte Carlo approach is adopted where the leaf water is assumed to reach steady state each day sometime between 13:00 and 18:00 local time. The leaf water isotopic ratio used for estimates of R_T in equations (2) and (4) was the average at each time step of all iterations of this Monte Carlo procedure.

Solving equation (5) requires knowledge of the isotopic ratio of the water used by the plants (i.e., R_{source}). Traditionally, this has been assumed to be equivalent to the isotopic ratio of the soil water weighted by the rooting depth. However, there is growing evidence to suggest that there is strong partitioning between bound and mobile soil waters with the former being more widely utilized by plants [*Brooks et al.*, 2010; *Good et al.*, 2015; *Evaristo et al.*, 2015; *Dawson and Ehleringer*, 1991]. Without an existing model to address this complexity, estimating the water used by plants must either come from direct measurements of the xylem water or adopting the assumption that plants draw on water which is isotopically equivalent to the bulk soil water. There was no regular sampling of soil, xylem, or leaf waters at US-NR1 during the period of this study, which increases the uncertainty of the T/ET analysis. The absence of regular sampling of these water pools made it difficult to model the isotopic ratio of the transpiration flux following the early part of the growing season when recent snowmelt was the dominant water source for the plants [*Hu et al.*, 2010]. In July and August, it is likely that the soil water pool contains a mixture of both summer rains and snowmelt that have both been modified isotopically by evaporation [*Mast et al.*, 1995]. Furthermore, the depth from which plants draw water from can be dynamic as the drying and rewetting of the soil make water available at different depths [*Hu et al.*, 2010]. To minimize these effects, we focused the analysis at US-NR1 only on the early part of the growing season when soils were saturated by snowmelt. We assumed that under these conditions the mobile and bound water sources would be well mixed, a condition which was not likely to be true later in the season when the soil column begins to dry [*Brooks et al.*, 2010].

Using an 11 year time series (1994–2004) of the isotopic ratio of the 1 April snowpack from the nearby Niwot SNOTEL site [*Anderson et al.*, 2015] and three additional years of the isotopic ratio of the snowpack (2004–2006) from *Hu et al.* [2010] (estimated from the published δD values), we calculated the average δ^{18}O for the snowpack at the site to be −20.7‰ with a standard error of 0.4‰. An analysis of soil moisture during the spring indicated that the soil moisture rapidly increased during this part of the season, suggesting percolation from melting snow was significantly larger than the evaporative flux. The xylem water measured by *Hu et al.* [2010] during a number of these years indicates an average value of ∼−16.5‰ (estimated from the published δD values). The xylem water is a few ‰ heavier than the average snowpack, which reflects either the presence of residual waters in the snowpack from the previous summer/fall and/or that the melt from the snowpack is preferentially heavier than the snowpack [*Mast et al.*, 1995; *Taylor et al.*, 2001; *Liu et al.*, 2004].

2.3.2.3. E and T Fluxes Estimates at MEF

The campaign at MEF included more regular sampling of soil, xylem, and leaf waters as reported by *Berkelhammer et al.* [2013], which provided input forcing for running an isotopic-enabled Land Surface Model (LSM) through the duration of the growing season. The use of an LSM addressed a number of the challenges associated with isotopic modifications of the snowpack and soil water during the course of the growing season. The model used was *isoLSM* [*Riley et al.*, 2002], which has previously been utilized in studies on the isotopic ratio of evaporation and transpiration fluxes [e.g., *Buenning et al.*, 2014; *Kanner et al.*, 2014; *Still et al.*, 2009]. The model was forced with air temperature, wind speed, pressure, incoming radiation, specific humidity, and precipitation rate, as well as the isotopic ratios (δ^{18}O and δD) of precipitation, the initial snowpack, and canopy vapor. A value of 1.2 m^2m^{-2} was used for the LAI (*P. Harley*, personal communication March 2013) and the physical properties of the soil (i.e., particle size distribution and hydraulic conductivity) were defined based on *Massman et al.* [2002]. The model uses the Richards equation to solve for the transport of soil water and was run with 20 soil layers. The rooting profile was defined using the approach of *Jackson et al.* [1996], where a rooting depth parameter describes the density of roots as a function of soil depth. A rooting depth parameter of 0.94 was used, which is typical for temperate evergreen forests. Root water uptake was considered nonfractionating. Because of relatively poor constraints on the resistances to moisture and heat transport (i.e., equations (A4), (A5) and (A7)–(A9) and the transpiration efficiency, an ensemble approach was adopted where these terms were varied uniformly within plausible ranges. From the 53,000 member ensemble, the simulations where latent heat, sensible heat, and total CO_2 fluxes produced a fit against the observations with a slope between 0.9 and 1.1 were retained (n = 112) and averaged together to provide a single time series for both R_T and R_E to be used for solving equation (2). The low success rate of generating realistic simulations was a product of the fact that the parameters were varied independently though they are, in fact, related to one another. This leads to a high probability of producing unrealistic parameter sets. The $\delta^{18}O_{ET}$ for MEF was obtained not from the model simulation but using equation (3) applied to the isotope and humidity profile data as described by *Berkelhammer et al.* [2013].

3. Results

3.1. Optimal Partitioning

In ecosystems with similar climate and plant functional types, the relationship between ET and GPP (once normalized to VPD) should yield similar functions [*Ball et al.*, 1987; *Zhou et al.*, 2016]. At MEF and US-NR1, the fits between between ET minima and GPP were not significantly different when considering the 95% confidence levels of the parameters used in the regression model (Figure 4c). This suggests that the normalization of GPP, binning, and minimization produced a function capturing the common stomatal control on water and carbon fluxes (Figure 4). The significant scatter apparent in Figures 4a and 4b results both from the uncertainty in the derivation of carbon and water fluxes and the presence of a significant amount of ET that cannot be explained simply in relation to GPP. Applying equation (1), the time-weighted average T/ET for MEF is 0.49 and 0.63 for US-NR1, though the data are bimodally distributed (Figure 6). Varying the cutoff frequency (which defines the threshold under which T/ET equals 1) between the 2nd–8th percentile, shifts the mean T/ET at both sites $\pm$0.05 (Figure 5), suggesting that the choice of this term does not impact the observation of a difference in T/ET between sites. Hourly T/ET is often between 0.90 and 1.0 at both sites, but there is a second population near 0.60 for US-NR1 and 0.30 for MEF. The T/ET cluster near 1 may partially be an artifact of the method, which requires that T/ET must be equal to 1 across the range of measured GPP values. However, values this high are not inconsistent with previous T/ET estimates of ~0.94 for the US-NR1 at midday during dry periods of the growing season [*Burns et al.*, 2015]. In addition, such values emerge independently in the isotope-derived T/ET data set from this site (section 3.2 and Figure 6).

To assess variations in T/ET on seasonal timescales, a daytime average is calculated for each site using all 15 years of data (1998–2013) at US-NR1 and the 2011 data from MEF (Figure 7a). During the 2011 growing season, when data are available from both sites, there is a significant correlation (Pearson's linear correlation of 0.68, $p \leq 0.00001$ and Spearman rank correlation coefficient of 0.72) between sites at the synoptic timescale (Figure 7b). The similarity between sites suggests that although differences in LAI may lead to a shift in the mean value of T/ET, the two respond similarly to weather systems and the associated effects on radiation, VPD, soil moisture/precipitation, and temperature. When an average seasonal cycle is calculated for US-NR1 by aggregating all 15 years of data, there is an absence of a growing season cycle in T/ET with the exception of low values (~0.40 relative to the average of 0.63) during the early part of the growing season when the trees

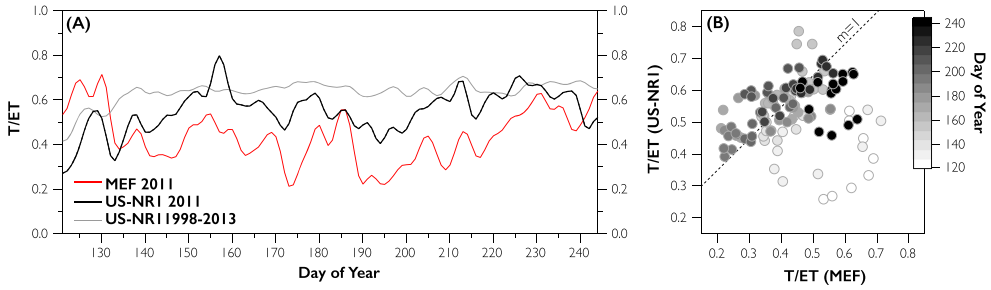

Figure 7. (a) Daytime-averaged T/ET using the data from Figure 4 for the MEF and US-NR1 sites for 2011 and for the entire period of the US-NR1 record. A 3 day sliding average was applied to daytime averages to accentuate the synoptic-scale variability. (b) Scatterplot showing the relationship between the 2011 T/ET for the MEF and US-NR1 sites after the sliding window average was applied. The color coding is day of the year and indicates that the fit between the two sites is strong when data from early in the season (i.e., day of the year ≤135) are excluded.

have not yet begun to actively transpire (Figure 7a). Growing season time-averaged T/ET values are calculated for each year using the same filtering procedures as described in section 2.3.1. There is a standard deviation on the annual averages of 0.04 (around an average of 0.6) with a minimum value of 0.54 observed in 2011 and a maximum of 0.66 observed in 2012. There is no statistically significant trend over the 15 years of data.

3.2. Isotope Partitioning

The isotopic ratio of the water vapor above the canopy at US-NR1 displays a strong seasonal cycle, varying between −40‰ in the winter and −10‰ in the summer (Figure 2). The range at MEF over the corresponding period of the year is similar, though slightly more enriched, as a consequence of both its more southerly latitude and lower altitude. The derived isotopic ratio of the ET flux ($\delta^{18}O_{ET}$) at both sites is systematically heavier than the background vapor ($\delta^{18}O_{Background}$) indicating a persistent source of isotopically heavy water from the canopy either from sublimation, evaporation, or transpiration (Figure 2). The offset between $\delta^{18}O_{ET}$ (equation (3)) and $\delta^{18}O_{Background}$ is not constant and does not covary systematically with temperature or VPD, which reflects both changes in the sources of the moisture flux (i.e., T and E) and in the fractionation factors' sensitivity to temperature, VPD, and turbulent conductances (Figure 8). However, at both sites we observed a sharp rise in $\delta^{18}O_{ET}$ under low VPD conditions that was not apparent in $\delta^{18}O_{Background}$ (Figure 8).

Applying equations (3) and (4), Figure 9 presents the distribution of hourly daytime (6:00–18:00) $\delta^{18}O$ of ET, T, and E for both the US-NR1 and MEF sites. The isotopic ratio of T at US-NR1 varies between −25‰ and 0‰, and was tightly distributed around the steady state flux derived from the estimates of the isotopic ratio of the xylem water. The values for T at MEF have a bimodal distribution that reflects a shift in the plants' reliance on an isotopically lighter water supply (∼−10‰) early in the growing season, followed by a transition toward the utilization of an isotopically heavier (∼−4‰) water source later in the season [*Berkelhammer et al.*, 2013]. The more complex distribution for the isotopic ratio of T at MEF relative to US-NR1 is attributable to the use

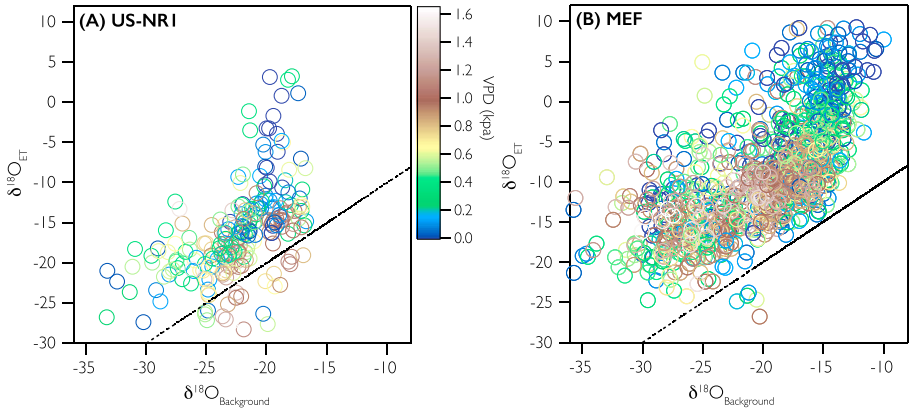

Figure 8. Scatterplots showing $\delta^{18}O_{Background}$ and $\delta^{18}O_{ET}$ using the data from Figure 2. Dotted line indicates the 1:1 line between the flux and background isotopic ratios. Color coding indicates the VPD associated with each data point and accentuates the divergence from the 1:1 line at low VPD values.

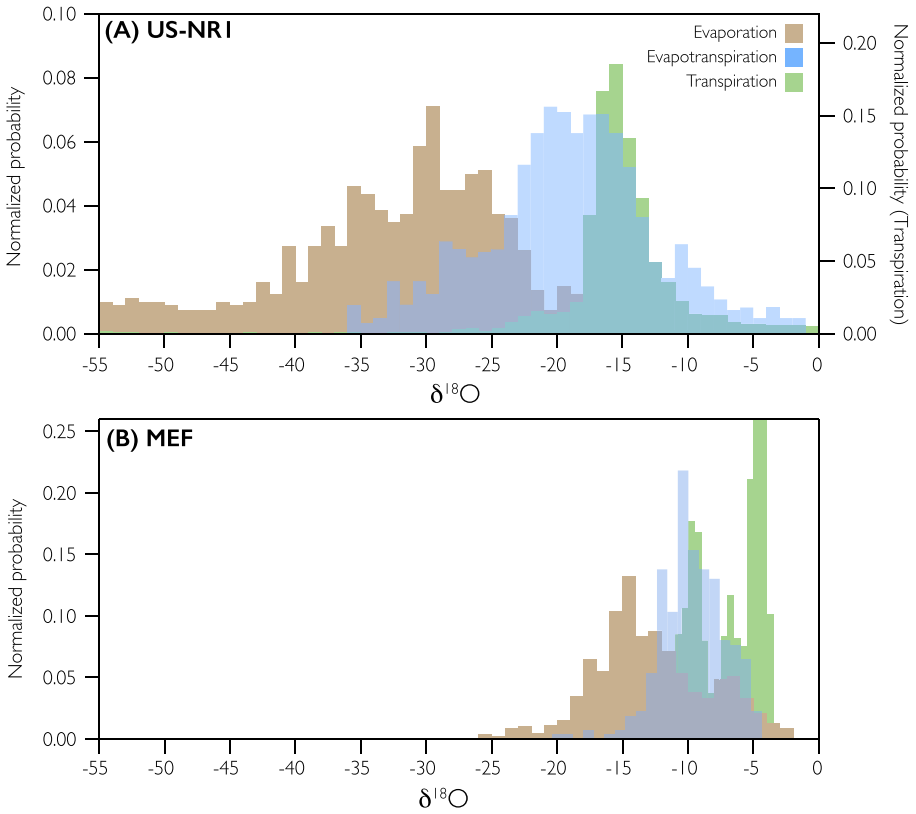

Figure 9. Normalized distributions of the $\delta^{18}O$ of ET (from tower profiles), transpiration, and evaporation (modeled) fluxes. A separate vertical scale for transpiration at US-NR1 is used because the distribution is significantly narrower than the other quantities.

of data from the entire growing season at MEF. The $\delta^{18}O_{ET}$ at both US-NR1 and MEF are largely constrained by the range of the T and E end-members; however, at US-NR1 there are a few brief windows when $\delta^{18}O_{ET}$ is isotopically heavier than T. These instances may arise from the presence of an additional isotopically heavy flux from the canopy (such as intercepted water) or may simply reflect the numerous sources of uncertainty in the method such as analytical uncertainty of individual isotopic measurements, application of the Keeling plot, and/or the modeling of the isotopic ratio of T or E [*Good et al.*, 2012].

Applying equation (2), we derive a distribution of T/ET for both sites yielding a time-average mean of 0.61 for US-NR1 and 0.50 for MEF (Figure 6). As with the optimal approach, the distribution at both sites is nonnormal with a peak between 0.90 and 1.0 and a lower peak at 0.60 for US-NR1 and 0.30 for MEF. The clustering of data near 1.0 partially reflects the presence of periodic solutions where T/ET was greater than 1.0, which were considered equivalent to 1.0. However, as noted in section 3.1, these T/ET values near 1.0 are consistent with those derived from the optimal approach.

4. Discussion

The methods presented here produced similar distributions of growing season hourly daytime T/ET at both the US-NR1 (LAI = 4.2) and MEF (LAI = 1.2) sites (Figures 1 and 6). Using a two-sample Kolmogorov-Smirnov test, we find that the methods produce similar bimodal distributions for T/ET at $p \leq 0.001$ for MEF and for US-NR1 at $p \leq 0.015$. Because the approaches were developed from independent theory, the agreement suggests that each was appropriate under these circumstances and are likely responding to similar ecohydrological processes. While the validity of the isotopic approach has previously been established [*Wang et al.*, 2010; *Yakir and Wang*, 1996], its application using an extended continuous time series in a field setting has rarely been attempted. The optimal approach, although based on the same theory established by *Scanlon and Kustas* [2010] and *Zhou et al.* [2016], is novel in its form and could easily be applied at most flux towers. Although the two methods display broad agreement, the root-mean-square difference between hourly T/ET

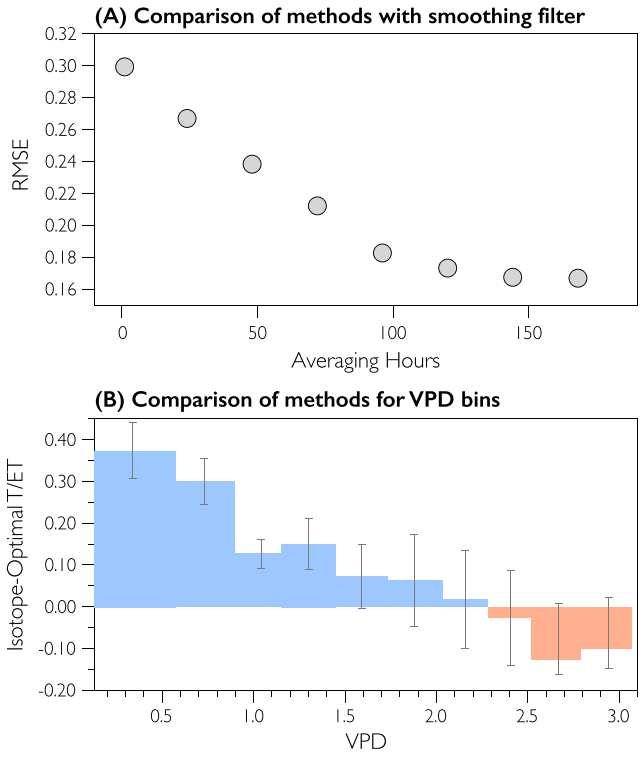

Figure 10. (a) Root-mean-square difference between partitioning approaches when smoothing filter of various lengths (1 through 168 h at 24 h intervals) is applied. (b) Residual between paired isotope- and optimal-derived T/ET values binned into 0.3 kpa VPD bins. Error bars are the standard error, and red (blue) bars are those bins where the isotope approach produces higher (lower) T/ET estimates than the optimal approach.

estimates is large (0.31). The size of the error relative to expected variations of T/ET indicates that the approaches are not reliable for estimates at the hourly timescale without further efforts to reduce uncertainty (some of which are discussed below). When a smoothing filter was applied (≥3 day) to both the isotopic and optimal T/ET time series, the root-mean-square difference was reduced to ≤0.2 (Figure 10a). It is on this temporal scale when most of the daytime growing season T/ET variability was found (Figure 7).

Some of the methodological differences arise from random analytical uncertainties in both eddy covariance [*Massman and Lee*, 2002] and stable isotopic measurements [*Bailey et al.*, 2015]. However, there is also a systematic offset between the optimal and isotopic approaches that emerges under conditions of low VPD (Figure 10b). When the air is nearly saturated, there is both increased exchange of leaf and canopy water and reduced atmospheric moisture demand. These competing influences on transpiration produce the "nonlinear effects of VPD on ET" referred to by *Beer et al.* [2009]. One explanation of the difference in T/ET between the isotopic and optimal approaches is the presence of a high T/ET bias in the isotopic approach when VPD is near 0. Under this condition, high stomatal conductance would facilitate isotopic exchange between the leaf water pool and canopy even when there is minimal transpiration [*Simonin et al.*, 2014]. While it has been shown in previous studies that this process can imprint the canopy vapor with anomalously low deuterium excess (δD-8·δ^{18}O) [*Berkelhammer et al.*, 2013], it is unclear that this process would enrich $\delta^{18}O_{ET}$ because low VPD would decrease transpiration and hinder the isotopic enrichment of the leaf water pool. A more viable explanation is that under conditions of low VPD, surface condensate including dew and intercepted water from previous precipitation events would be prevalent. The evaporation or exchange of these waters would lead to an isotopically enriched flux, which may explain the steep rise in $\delta^{18}O_{ET}$ as VPD approaches 0. Thus, we offer the possibility that the high bias in isotopically derived T/ET during humid conditions may emerge from the enrichment of $\delta^{18}O_{ET}$ due to the presence of a liquid water pool in the canopy.

An alternative explanation, though not mutually exclusive, is the presence of a low bias in the optimal approach under conditions of high humidity. Assuming that there is no systematic error in the flux estimates at high humidity or an error in the GPP flux partitioning, the likely alternative source of a bias would

manifest in how the effect of VPD on stomatal conductance was accounted for when generating the ET minimum curve (Figure 4). Multiplying GPP by VPD is intended to maximize the fit between GPP and ET because it accentuates the stomatal response to VPD. However, this approach assumes a monotonic response of stomatal conductance to VPD. This assumption is valid under high VPD (low humidity) conditions, but when VPD is low (i.e., $\leq$1 kPa), the response of stomatal conductance to VPD becomes significantly weaker, and the slope can reverse direction [*Day*, 2000; *Addington et al.*, 2004; *Ocheltree et al.*, 2014]. By not accounting for this nonmonotonic behavior, the approach underestimates T and could generate a bias in T/ET under low VPD conditions.

Although we are not able to isolate the process leading to divergence between the two T/ET approaches at high humidity, the observation highlights a set of ecohydrological processes that are not well characterized. These processes may include interception and dew fluxes, which are difficult to observe but can be of a significant magnitude [*Good et al.*, 2015]. In addition, while the stomatal response to humidity stress has been generally well characterized [*Ball et al.*, 1987], the apparent nonlinear behavior of the stomata under nearly saturated conditions is poorly constrained. In the temperate needle leafed environments discussed here, these processes may not be critical as daytime conditions generally are associated with relatively high VPD and surface waters are not likely to remain present for long periods of time. However, in extending this type of analysis to tropical and boreal systems, these processes will become more important.

In terms of absolute skill, it is not apparent which of the two methods is preferable. Currently, there is no agreed-upon benchmark method at the plot scale to assess whether discrepancies between methods are the result of a bias in one or both of the methods. From a practical standpoint, the optimal approach can be derived through more widely available data sets [*Zhou et al.*, 2016]. However, the optimal approach relies on the assumption that transpiration must periodically be the dominant flux, which may negate its utility in ecosystems where there is always sufficient soil or surface water to support a significant evaporation flux. The isotope approach, on the other hand, can be applied without any maximum T/ET condition being met. However, because of the difficulties in estimating the isotopic ratio of the ET flux from the Keeling plot approach, as well as the analytical difficulty of making these measurements [*Good et al.*, 2012], it is a technique that cannot be easily implemented. Furthermore, because the interception flux is likely to be isotopically heavier than E but abiotic, it can generate a high bias in the T/ET estimate. The failure to properly account for this term has already been shown to be problematic [*Good et al.*, 2015; *Schlesinger and Jasechko*, 2014].

One advance toward adoption of the isotopic approach would be the development of techniques to acquire continuous in situ measurements of xylem and soil water isotopic ratios [e.g., *Rothfuss et al.*, 2015]. At the US-NR1 site, the required assumptions regarding continuity of snow, soil, and xylem water isotopic ratios prohibited analyzing T/ET over the entire growing season. However, the relative similarity with the optimal approach validates that certain simplifying assumptions regarding seasonal plant water use may have only minor impacts on the derivation of T/ET. These assumptions are tolerable because $\delta^{18}O_{ET}$ is, on its own, a sensitive indicator of T/ET. The sensitivity of $\delta^{18}O_{ET}$ to variations in T/ET, without highly specific knowledge of leaf and soil processes, has justified global and regional estimates of transpiration from satellite retrievals of water isotopes [*Worden et al.*, 2007; *Risi et al.*, 2013; *Frankenberg et al.*, 2009; *Good et al.*, 2015]. The results presented here circumstantially support the use of large-scale patterns in water vapor isotopic ratios to track continental moisture sources. At MEF, recurrent sampling of soil and xylem waters provided necessary constraints to extend the analysis through the growing season and use a LSM to manage the complexity associated with modification of the isotopic ratio of soil water across the growing season [*Kanner et al.*, 2014]. However, the data at MEF, despite use of the LSM, did not agree better with the optimal approach than at US-NR1. This result similarly suggests that $\delta^{18}O_{ET}$ is a useful tracer of T/ET even in the absence of strong constraints on the isotopic ratios of the E and T sources.

Utilizing all available data from both approaches, we arrive at a time-averaged T/ET estimate of 0.49 $\pm$ 0.23 and 0.62 $\pm$ 0.27 for MEF and US-NR1, respectively (Figure 6e). The analysis is based on only daytime data (6:00–18:00) and data from time periods when GPP was greater than 0 and therefore excludes the fact that ecosystems may lose water at night. The values are significantly lower than a recent estimate of 0.94 for US-NR1 by *Burns et al.* [2015], who used the regression between VPD and ET to arrive at the E component of ET. However, the average from *Burns et al.* [2015] was generated using only data from dry periods and during midday. Under such conditions, it is expected that T would predominate given the presence of water stored in trees and access to deeper water from the root systems that would not be available for E. In addition,

it can be assumed that under these conditions, interception would be negligible. In their analysis, *Burns et al.* [2015] note that following precipitation events, the presence of available surface waters lead to a significant reduction of T/ET on the order of 10–20%. The difference observed between the estimate of 0.62 (Figure 6) and 0.94 from *Burns et al.* [2015], is consistent with the difference in global T/ET estimates between *Jasechko et al.* [2013] and *Good et al.* [2015] when interception was increased from 7 to 27% and thus may represent the evaporation of intercepted and surface waters at US-NR1 [*Molotch et al.*, 2007].

The mean values for each site are close to those derived using the global fit between LAI and T/ET from *Wang et al.* [2014] (0.40 and 0.60, respectively). However, the total distribution of hourly T/ET data, which includes diel, synoptic, and seasonal variability is not normal and suggests that the mean value is not a good predictor of T/ET at any timescale other than seasonal. Despite the complex controls on T/ET, there was a significant agreement ($p \leq 0.0001$) between synoptic-scale variability at US-NR1 and MEF (Figure 7). Variability of T/ET on these timescales can shift by a factor of 2 over 2–3 days. Because these are evergreen sites and there is limited variability in LAI, the variability must arise from the biotic and abiotic response to weather and soil moisture dynamics. Thus, studies of T/ET on the watershed scale, such as *Jasechko et al.* [2013], or using regional atmospheric data, such as *Good et al.* [2015], are likely to capture regionally relevant information. Surprisingly, the synoptic-scale variability is larger than the average seasonal cycle, with the exception of low values during the very early period of the growing season when soils are saturated and the snowpack is melting but photosynthetically active radiation and air temperatures are relatively low. The lack of a seasonal cycle, in spite of high-amplitude temperature and VPD seasonal cycles, highlights that T/ET is very likely set by LAI [*Wang et al.*, 2014], which is relatively invariant over a single growing season.

The factors that stabilize T/ET over short timescales (for example, LAI) can experience shifts on interannual and longer timescales associated with tree mortality, greening associated with higher atmospheric CO_2, changes in snowpack dynamics or shifts in the root:shoot ratio. Using a 15 year time series of time-weighted annually averaged T/ET at US-NR1, we find relatively stable values (standard deviation of 0.04) and the absence of any secular trend. Over this time period, 2011 emerges as the year with the singularly lowest T/ET (0.55), whereas 2012 had the highest T/ET (0.66). Using Moderate Resolution Imaging Spectroradiometer (MODIS)-derived LAI for a 0.1° radius around US-NR1 [*Xiao et al.*, 2014], we observe that 2011 and 2012 were associated with the lowest (2.1) and highest (2.6) LAI values since 2001. We note, however, that there is a significant offset between LAI observed at US-NR1 (4.2) and that derived from MODIS (2.3). This may be due to grid cell averaging, but for purposes of this study we focus only on the interannual variability as opposed to potential biases in the mean retrieval for this site. Nonetheless, the result suggests temporal variations in T/ET are associated with changes in LAI, which would enable spatiotemporal projections of T/ET using global LAI products. However, we note that while end-member LAI values, as in 2011 and 2012, were associated with shifts in T/ET, this relationship was not stable through the record and there was no statistically significant regression between the two. There are many other factors potentially driving temporal variations in T/ET, which make it difficult to argue for LAI causality. For example, 2011 was the largest snowpack over the last 15 years at US-NR1, which lead to a late melting season that would have contributed to a proportionately larger increase in E relative to T.

5. Conclusion

Although T/ET is a fundamental ecosystem property, a unified approach to derive its variability at the plot scale has yet to be established. In montane ecosystems, the combination of changes in the timing of snowmelt, length of the growing season, rising CO_2, and rising VPD (a consequence of warming) [*Barnett et al.*, 2005; *Williams et al.*, 2013; *Pepin et al.*, 2015] has the potential to shift how latent heat flux is distributed between biotic and abiotic processes. In order to anticipate these shifts, which could have consequences for surface and subsurface hydrological dynamics and ecosystem productivity, LSMs run with realistic future forcing scenarios would be needed. However, the lack of observational constraints on T/ET has made it impossible to diagnose whether LSMs can accurately distribute the terrestrial latent heat budget.

In this study, two plot-scale approaches to derive T/ET are adopted: (1) the optimal approach, which comes from established theory on the shared stomatal control of water and carbon fluxes and (2) the isotopic approach, which relies on the difference between the isotopic ratio of transpiration and evaporation fluxes. Despite high uncertainty on hourly derived T/ET values, the independent approaches yield nearly identical distributions and strong agreement on the synoptic timescale. The work is distinct from previous studies in that the estimates are derived from independent but same-scale approaches at two sites with measurably

different T/ET values. The results indicate that T/ET values vary across the entire 0–1 spectrum on hourly timescales (0.2–0.8 on synoptic timescales) at both sites, with time-averaged mean values of 0.49 at the low LAI (1.2) site and 0.62 at the high LAI (4.2) site. These values fall within the expected ranges based on previous global analyses of T/ET [*Schlesinger and Jasechko*, 2014; *Good et al.*, 2015; *Wang et al.*, 2014] but highlight the presence of bimodal T/ET distributions at both sites. The existence of both a high and low T/ET population may reflect the temporary availability of surface water pools, including intercepted precipitation, which increase the abiotic component (i.e., E) of the latent heat flux. Therefore, snapshots of T/ET based on short campaigns cannot provide an universally applicable value for an ecosystem.

At US-NR1, there was no measurable long-term trend in T/ET, implying the factors controlling the partitioning of the latent heat flux have remained stable. This could be due to the fact that changes in T/ET are yet too subtle to be measurable or that any changes in T have been associated with proportionate changes in E. One implication of this finding is that the use of ET, as opposed to T, when calculating water use efficiency would not inherently generate a trend in the data. This is relevant in light of the observed global increase in water use efficiency and efforts to isolate the process(es) driving this trend [*Keenan et al.*, 2013; *Frank et al.*, 2015]. Similar analyses at other sites would be necessary to establish whether T/ET has remained stable elsewhere in spite of the increase in T [*Frank et al.*, 2015] and water use efficiency. If no trend in T/ET is apparent, it suggests the presence of ecohydrological feedbacks that maintain coupling between T and E.

To deploy these approaches in boreal or tropical ecosystems, future work is needed to address the discrepancy between methods that emerged at high humidity. If the discrepancy can be addressed through, for example, better constraints on xylem and soil water isotopic ratios and the stomatal response to high humidity, greater confidence can be assigned to the optimal approach and this can be adopted with confidence across global flux sites [*Zhou et al.*, 2016]. This would allow reanalysis of T/ET using extended eddy covariance time series, which would enable analysis of interannual trends that might be associated with the stomatal response to rising atmospheric CO_2 or changes in the length or timing of the growing season [*Keenan et al.*, 2013; *Frank et al.*, 2015]. Such analyses would also provide better constraints on the sensitivity of T/ET to LAI, which could be utilized along with remotely sensed LAI products to generate global T/ET estimates.

Appendix A: Canopy Kinetic Fractionation Factor

The kinetic fractionation factor for transpiration, $\epsilon_{\text{transpiration}}$, is calculated from equation (A1) based on *Lee et al.* [2009]:

$$\epsilon_{\text{transpiration}} = \frac{21g^{-1}_{\text{boundary}} + 32g^{-1}_{\text{canopy}}}{g^{-1}_{\text{atmosphere}} + g^{-1}_{\text{boundary}} + g^{-1}_{\text{canopy}}} \tag{A1}$$

The kinetic fractionation factor for evaporation, $\epsilon_{\text{evaporation}}$, is calculated from equation (A2) based on *Lee et al.* [2009]:

$$\epsilon_{\text{evaporation}} = \frac{32g^{-1}_{\text{soil}}}{g^{-1}_{\text{atmosphere}} + g^{-1}_{\text{subcanopy}} + g^{-1}_{\text{soil}}} \tag{A2}$$

ϵ is related to the fractionation factor α using equation (A3):

$$\alpha = \frac{\epsilon}{1000} + 1 \tag{A3}$$

The aerodynamic conductance for air within the canopy is calculated as follows:

$$g^{-1}_{\text{canopy}} = \frac{\text{VPD}}{\text{ET}} + g^{-1}_{\text{total}} \cdot \frac{H}{\text{ET}} \cdot [s - 1]. \tag{A4}$$

ET is the water flux in g H_2O m^{-2} s^{-1} (converted from the mole fraction), s is the slope of saturated water vapor pressure and temperature, H is kinematic heat flux, and g_{total} is derived using equation (A5):

$$g^{-1}_{\text{total}} = \frac{1}{u \cdot Tc}, \tag{A5}$$

where u is wind speed at the reference height (21.5 m) and Tc is the transfer coefficient derived from equation (A6):

$$Tc = \frac{k^2}{\log(z_m - d)/z_o - \phi_{\text{momentum}} \cdot \log(z_m - d)/z_q - \phi_{\text{heat}}} \tag{A6}$$

where k is the Von Karman constant, z_m is the reference height (21.5 m), d is the displacement height, z_o is the momentum roughness, z_q is the humidity roughness, and $\phi_{h/m}$ are the integral similarity functions for heat and momentum.

The boundary layer conductance is derived from equation (A7):

$$g_{\text{boundary}}^{-1} = \frac{b}{2} \cdot L \cdot \frac{l_w}{u}^{0.5} \tag{A7}$$

where b is the boundary layer resistance coefficient, L is the leaf area index, l_w is the leaf dimension, and u is the wind speed. The atmospheric conductance is taken as the residual between the total (equation (A5)) and boundary layer (equation (A7)) conductances:

$$g_{\text{atmosphere}}^{-1} = g_{\text{boundary}}^{-1} - g_{\text{total}}^{-1} \tag{A8}$$

For estimation of $\epsilon_{\text{evaporation}}$, the resistance within the canopy air space must be estimated which is done using equation (A9):

$$g_{\text{subcanopy}}^{-1} = \int_0^{\text{canopy}} \frac{dz}{K} \tag{A9}$$

where K is eddy diffusivity with units of $m^2\ s^{-1}$, dz is the length of the canopy air space, and the integral is calculated from the soil surface across the canopy air space. g_{soil}^{-1} is assumed to have a constant value of 500 s m^{-1} [*Lee et al.*, 2009].

Acknowledgments
This work was partially supported by NSF grant AGS-0955841 to D.C.N., NSF grant AGS-1502776 to M.B., and NSF grant EAR-0423662 to M.W.W. The authors acknowledge D. Bowling for field assistance and feedback on an earlier version of the manuscript. The water isotope data and associated climate and eddy covariance data for the US-NR1 site site are available here: urquell.colorado.edu/data_ameriflux/data_30min/. Data from the MEF site are available from the author (berkelha@uic.edu) upon request.

References

Addington, R. N., R. J. Mitchell, R. Oren, and L. A. Donovan (2004), Stomatal sensitivity to vapor pressure deficit and its relationship to hydraulic conductance in Pinus palustris, *Tree Physiol.*, *24*(5), 561–569.
Allison, G., and C. Barnes (1983), Estimation of evaporation from non-vegetated surfaces using natural deuterium, *Nature*, *301*(5896), 143–145.
Anderson, L., M. Berkelhammer, and M. A. Mast (2015), Isotopes in North American Rocky Mountain snowpack 1993–2014, *Quat. Sci. Rev.*, *131*, 262–273.
Bailey, A., D. Noone, M. Berkelhammer, H. C. Steen-Larsen, and P. Sato (2015), The stability and calibration of water vapor isotope ratio measurements during long-term deployments, *Atmos. Meas. Tech.*, *8*(10), 4521–4538.
Ball, J. T., I. E. Woodrow, and J. A. Berry (1987), A model predicting stomatal conductance and its contribution to the control of photosynthesis under different environmental conditions, in *Progress in Photosynthesis Research*, edited by J. Biggins, pp. 221–224, Springer, Netherlands.
Barbour, M. M., J. S. Roden, G. D. Farquhar, and J. R. Ehleringer (2004), Expressing leaf water and cellulose oxygen isotope ratios as enrichment above source water reveals evidence of a Péclet effect, *Oecologia*, *138*(3), 426–435.
Barnett, T. P., J. C. Adam, and D. P. Lettenmaier (2005), Potential impacts of a warming climate on water availability in snow-dominated regions, *Nature*, *438*(7066), 303–309.
Beer, C., et al. (2009), Temporal and among-site variability of inherent water use efficiency at the ecosystem level, *Global Biogeochem. Cycles*, *23*, GB2018, doi:10.1029/2008GB003233.
Berkelhammer, M., J. Hu, A. Bailey, D. C. Noone, C. J. Still, H. Barnard, D. Gochis, G. S. Hsiao, T. Rahn, and A. Turnipseed (2013), The nocturnal water cycle in an open-canopy forest, *J. Geophys. Res. Atmos.*, *118*, 10,225–10,242, doi:10.1002/jgrd.50701.
Blanken, P. D., M. W. Williams, S. P. Burns, R. K. Monson, J. Knowles, K. Chowanski, and T. Ackerman (2009), A comparison of water and carbon dioxide exchange at a windy alpine tundra and subalpine forest site near Niwot Ridge, Colorado, *Biogeochemistry*, *95*(1), 61–76.
Bowling, D., A. P. Ballantyne, J. Miller, S. Burns, T. Conway, O. Menzer, B. Stephens, and B. Vaughn (2014), Ecological processes dominate the ^{13}C land disequilibrium in a Rocky Mountain subalpine forest, *Global Biogeochem. Cycles*, *28*, 352–370, doi:10.1002/2013GB004686.
Brooks, J. R., H. R. Barnard, R. Coulombe, and J. J. McDonnell (2010), Ecohydrologic separation of water between trees and streams in a Mediterranean climate, *Nat. Geosci.*, *3*(2), 100–104.
Buenning, N., D. Noone, J. Randerson, W. J. Riley, and C. Still (2014), The response of the $^{18}O/^{16}O$ composition of atmospheric CO_2 to changes in environmental conditions, *J. Geophys. Res. Biogeosci.*, *119*, 55–79, doi:10.1002/2013JG002312.
Burns, S., P. Blanken, A. Turnipseed, J. Hu, and R. Monson (2015), The influence of warm-season precipitation on the diel cycle of the surface energy balance and carbon dioxide at a Colorado subalpine forest site, *Biogeosciences*, *12*, 7349–7377.
Coplen, T. B. (1988), Normalization of oxygen and hydrogen isotope data, *Chem. Geol.*, *72*(4), 293–297.
Craig, H., and L. Gordon (1965), Deuterium and ^{18}O variations in the ocean and the marine atmosphere, in *Stable Isotopes in Oceanographic Studies and Paleotemperatures, Spoleto*, vol. 9, edited by E. Tongiorgi, pp. 9–130, Laboratorio di Geologia Nucleare, Pisa, Italy.
Dawson, T. E., and J. R. Ehleringer (1991), Streamside trees that do not use stream water, *Nature*, *350*(6316), 335–337.
Day, M. E. (2000), Influence of temperature and leaf-to-air vapor pressure deficit on net photosynthesis and stomatal conductance in red spruce (Picea rubens), *Tree Physiol.*, *20*(1), 57–63.
Dubbert, M., M. Cuntz, A. Piayda, and C. Werner (2014), Oxygen isotope signatures of transpired water vapor: The role of isotopic non-steady-state transpiration under natural conditions, *New Phytol.*, *203*(4), 1242–1252.
Dunn, S., and R. Mackay (1995), Spatial variation in evapotranspiration and the influence of land use on catchment hydrology, *J. Hydrol.*, *171*(1), 49–73.
Evaristo, J., S. Jasechko, and J. J. McDonnell (2015), Global separation of plant transpiration from groundwater and streamflow, *Nature*, *525*(7567), 91–94.
Falge, E., et al. (2001), Gap filling strategies for long term energy flux data sets, *Agric. For. Meteorol.*, *107*(1), 71–77.

Farley, K., E. Jobbágy, and R. Jackson (2005), Effects of afforestation on water yield: A global synthesis with implications for policy, *Global Change Biol.*, *11*(10), 1565–1576.
Frank, D., et al. (2015), Water-use efficiency and transpiration across european forests during the anthropocene, *Nat. Clim. Change*, *5*(6), 579–583.
Frankenberg, C., et al. (2009), Dynamic processes governing lower-Tropospheric HDO/H_2O ratios as observed from space and ground, *Science*, *325*(5946), 1374–1377.
Good, S. P., K. Soderberg, L. Wang, and K. K. Caylor (2012), Uncertainties in the assessment of the isotopic composition of surface fluxes: A direct comparison of techniques using laser-based water vapor isotope analyzers, *J. Geophys. Res.*, *117*, D15301, doi:10.1029/2011JD017168.
Good, S. P., K. Soderberg, K. Guan, E. G. King, T. M. Scanlon, and K. K. Caylor (2014), δ^2h isotopic flux partitioning of evapotranspiration over a grass field following a water pulse and subsequent dry down, *Water Resour. Res.*, *50*, 1410–1432, doi:10.1002/2013WR014333.
Good, S. P., D. Noone, and G. Bowen (2015), Hydrologic connectivity constrains partitioning of global terrestrial water fluxes, *Science*, *349*(6244), 175–177.
Gupta, P., D. Noone, J. Galewsky, C. Sweeney, and B. H. Vaughn (2009), Demonstration of high-precision continuous measurements of water vapor isotopologues in laboratory and remote field deployments using wavelength-scanned cavity ring-down spectroscopy (WS-CRDS) technology, *Rapid Commun. Mass Spectrom.*, *23*(16), 2534–2542.
Horita, J., and D. J. Wesolowski (1994), Liquid-vapor fractionation of oxygen and hydrogen isotopes of water from the freezing to the critical temperature, *Geochim. Cosmochim. Acta*, *58*(16), 3425–3437.
Hu, J., D. J. Moore, S. P. Burns, and R. K. Monson (2010), Longer growing seasons lead to less carbon sequestration by a subalpine forest, *Global Change Biol.*, *16*(2), 771–783.
Jackson, R., J. Canadell, J. R. Ehleringer, H. Mooney, O. Sala, and E. Schulze (1996), A global analysis of root distributions for terrestrial biomes, *Oecologia*, *108*(3), 389–411.
Jasechko, S., Z. D. Sharp, J. J. Gibson, S. J. Birks, Y. Yi, and P. J. Fawcett (2013), Terrestrial water fluxes dominated by transpiration, *Nature*, *496*(7445), 347–350.
Johnson, L., Z. Sharp, J. Galewsky, M. Strong, A. Van Pelt, F. Dong, and D. Noone (2011), Hydrogen isotope correction for laser instrument measurement bias at low water vapor concentration using conventional isotope analyses: Application to measurements from Mauna Loa Observatory, Hawaii, *Rapid Commun. Mass Spectrom.*, *25*(5), 608–616.
Johnson, W. (1956), The effect of grazing intensity on plant composition, vigor, and growth of pine-bunchgrass ranges in central Colorado, *Ecology*, *37*(4), 790–798.
Kanner, L. C., N. H. Buenning, L. D. Stott, A. Timmermann, and D. Noone (2014), The role of soil processes in δ^{18}O terrestrial climate proxies, *Global Biogeochem. Cycles*, *28*(3), 239–252, doi:10.1002/2013GB004742.
Keenan, T. F., D. Y. Hollinger, G. Bohrer, D. Dragoni, J. W. Munger, H. P. Schmid, and A. D. Richardson (2013), Increase in forest water-use efficiency as atmospheric carbon dioxide concentrations rise, *Nature*, *499*(7458), 324–327.
Knowles, J. F., A. Harpold, R. Cowie, M. Zeliff, H. Barnard, S. Burns, P. Blanken, J. Morse, and M. Williams (2015a), The relative contributions of alpine and subalpine ecosystems to the water balance of a mountainous, headwater catchment, *Hydrol. Processes*, *29*(22), 4794–4808.
Knowles, J. F., S. P. Burns, P. D. Blanken, and R. K. Monson (2015b), Fluxes of energy, water, and carbon dioxide from mountain ecosystems at Niwot Ridge, Colorado, *Plant Ecolog. Divers.*, *8*(5–6), 663–676, doi:10.1080/17550874.2014.904950.
Kool, D., N. Agam, N. Lazarovitch, J. Heitman, T. Sauer, and A. Ben-Gal (2014), A review of approaches for evapotranspiration partitioning, *Agric. For. Meteorol.*, *184*, 56–70.
Kuglitsch, F., et al. (2008), Characterisation of ecosystem water-use efficiency of European forests from eddy covariance measurements, *Biogeosci. Discuss.*, *5*(6), 4481–4519.
Law, B., et al. (2002), Environmental controls over carbon dioxide and water vapor exchange of terrestrial vegetation, *Agric. For. Meteorol.*, *113*(1), 97–120.
Lee, J. H., X. H. Feng, E. S. Posmentier, A. M. Faiia, and S. Taylor (2009), Stable isotopic exchange rate constant between snow and liquid water, *Chem. Geol.*, *260*(1–2), 57–62.
Liu, F., M. W. Williams, and N. Caine (2004), Source waters and flow paths in an alpine catchment, Colorado Front Range, United States, *Water Resour. Res.*, *40*, W09401, doi:10.1029/2004WR003076.
Massman, W., and X. Lee (2002), Eddy covariance flux corrections and uncertainties in long-term studies of carbon and energy exchanges, *Agric. For. Meteorol.*, *113*(1), 121–144.
Massman, W., J. Frank, W. Shepperd, M. Platten, P. N. Omi, and L. A. Joyce (2002), In situ soil temperature and heat flux measurements during controlled surface burns at a southern Colorado forest site, in *Fire, Fuel, Treatments and Ecological Restoration*, edited by P. N. Omi and L.A. Joyce, pp. 69–87, U.S. Dep. of Agric., For. Serv., Rocky Mt. Res. Station, Fort Collins, Colo.
Mast, M. A., C. Kendall, D. H. Campbell, D. W. Clow, and J. Back (1995), Determination of hydrologic pathways in an alpine-subalpine basin using isotopic and chemical tracers, Loch Vale Watershed, Colorado, USA, in *IAHS Publications-Series of Proceedings and Reports-Intern Assoc Hydrological Sciences*, vol. 228, edited by K. A. Tonnesson, M. W. Williams, and M. Tranter, pp. 263–270, Inst. of Hydrol., Wallingford, Oxfordshire.
Miller, J. B., and P. P. Tans (2003), Calculating isotopic fractionation from atmospheric measurements at various scales, *Tellus B*, *55*(2), 207–214.
Molotch, N. P., P. D. Blanken, M. W. Williams, A. A. Turnipseed, R. K. Monson, and S. A. Margulis (2007), Estimating sublimation of intercepted and sub-canopy snow using eddy covariance systems, *Hydrol. Processes*, *21*(12), 1567–1575.
Monson, R., A. Turnipseed, J. Sparks, P. Harley, L. Scott-Denton, K. Sparks, and T. Huxman (2002), Carbon sequestration in a high-elevation, subalpine forest, *Global Change Biol.*, *8*(5), 459–478.
Monteith, J. (1981), Evaporation and surface temperature, *Q. J. R. Meteorol. Soc.*, *107*(451), 1–27.
Moreira, M., L. Sternberg, L. Martinelli, R. Victoria, E. Barbosa, L. Bonates, and D. Nepstad (1997), Contribution of transpiration to forest ambient vapour based on isotopic measurements, *Global Change Biol.*, *3*, 439–450.
Noone, D., et al. (2013), Determining water sources in the boundary layer from tall tower profiles of water vapor and surface water isotope ratios after a snowstorm in Colorado, *Atmos. Chem. Phys.*, *13*(3), 1607–1623.
Ocheltree, T., J. Nippert, and P. Prasad (2014), Stomatal responses to changes in vapor pressure deficit reflect tissue-specific differences in hydraulic conductance, *Plant Cell Environ.*, *37*(1), 132–139.
Ortega, J., et al. (2014), Overview of the Manitou Experimental Forest Observatory: Site description and selected science results from 2008 to 2013, *Atmospheric Chemistry and Physics*, *14*(12), 6345–6367.
Oyler, J. W., S. Z. Dobrowski, A. P. Ballantyne, A. E. Klene, and S. W. Running (2015), Artificial amplification of warming trends across the mountains of the western United States, *Geophys. Res. Lett.*, *42*, 153–161, doi:10.1002/2014GL062803.

Pepin, N., et al. (2015), Elevation-dependent warming in mountain regions of the world, *Nat. Clim. Change*, *5*, 424–430.
Reichstein, M., et al. (2005), On the separation of net ecosystem exchange into assimilation and ecosystem respiration: Review and improved algorithm, *Global Change Biol.*, *11*(9), 1424–1439.
Reichstein, M., P. C. Stoy, A. R. Desai, G. Lasslop, and A. D. Richardson (2012), Partitioning of net fluxes, in *Eddy Covariance*, edited by M. Aubinet, T. Vesala, and D. Papale, pp. 263–289, Springer, Netherlands.
Riley, W., C. Still, M. Torn, and J. Berry (2002), A mechanistic model of $H_2^{18}O$ and $C^{18}OO$ fluxes between ecosystems and the atmosphere: Model description and sensitivity analyses, *Global Biogeochemical Cycles*, *16*(4), 1095, doi:10.1029/2002GB001878.
Risi, C., D. Noone, C. Frankenberg, and J. Worden (2013), Role of continental recycling in intraseasonal variations of continental moisture as deduced from model simulations and water vapor isotopic measurements, *Water Resour. Res.*, *49*, 4136–4156, doi:10.1002/wrcr.20312.
Rothfuss, Y., S. Merz, J. Vanderborght, N. Hermes, A. Weuthen, A. Pohlmeier, H. Vereecken, and N. Brüggemann (2015), Long-term and high-frequency non-destructive monitoring of water stable isotope profiles in an evaporating soil column, *Hydrol. Earth Syst. Sci.*, *19*(10), 40,67–40,80.
Scanlon, T. M., and W. P. Kustas (2010), Partitioning carbon dioxide and water vapor fluxes using correlation analysis, *Agric. For. Meteorol.*, *150*(1), 89–99.
Schlesinger, W. H., and S. Jasechko (2014), Transpiration in the global water cycle, *Agric. For. Meteorol.*, *189*, 115–117.
Schmidt, M., K. Maseyk, C. Lett, P. Biron, P. Richard, T. Bariac, and U. Seibt (2010), Concentration effects on laser-based $\delta^{18}O$ and $\delta^{2}H$ measurements and implications for the calibration of vapour measurements with liquid standards, *Rapid Commun. Mass Spectrom.*, *24*(24), 3553–3561.
Seibt, U., L. Wingate, J. Berry, and J. Lloyd (2006), Non-steady state effects in diurnal ^{18}O discrimination by Picea sitchensis branches in the field, *Plant Cell Environ.*, *29*(5), 928–939.
Serreze, M. C., M. P. Clark, R. L. Armstrong, D. A. McGinnis, and R. S. Pulwarty (1999), Characteristics of the western United States snowpack from snowpack telemetry (SNOTEL) data, *Water Resour. Res.*, *35*(7), 2145–2160.
Simonin, K. A., P. Link, D. Rempe, S. Miller, J. Oshun, C. Bode, W. E. Dietrich, I. Fung, and T. E. Dawson (2014), Vegetation induced changes in the stable isotope composition of near surface humidity, *Ecohydrology*, *7*(3), 936–949.
Still, C., et al. (2009), Influence of clouds and diffuse radiation on ecosystem-atmosphere CO_2 and $CO^{18}O$ exchanges, *J. Geophys. Res.*, *114*, G01018, doi:10.1029/2007JG000675.
Sutanto, S., B. Van den Hurk, P. Dirmeyer, S. Seneviratne, T. Rockmann, K. Trenberth, E. Blyth, J. Wenninger, and G. Hoffmann (2014), HESS opinions: A perspective on isotope versus non-isotope approaches to determine the contribution of transpiration to total evaporation, *Hydrol. Earth Syst. Sci.*, *18*(8), 2815–2827.
Taylor, S., X. Feng, J. Kirchner, R. Osterhuber, B. Klaue, and C. Renshaw (2001), Isotopic evolution of a seasonal snowpack and its melt, *Water Resour. Res.*, *37*(3), 759–769.
Turnipseed, A., P. Blanken, D. Anderson, and R. Monson (2002), Energy budget above a high-elevation subalpine forest in complex topography, *Agric. For. Meteorol.*, *110*(3), 177–201.
Wang, L., K. K. Caylor, J. C. Villegas, G. A. Barron-Gafford, D. D. Breshears, and T. E. Huxman (2010), Partitioning evapotranspiration across gradients of woody plant cover: Assessment of a stable isotope technique, *Geophys. Res. Lett.*, *37*, L09401, doi:10.1029/2010GL043228.
Wang, L., S. P. Good, and K. K. Caylor (2014), Global synthesis of vegetation control on evapotranspiration partitioning, *Geophys. Res. Lett.*, *41*, 6753–6757, doi:10.1002/2014GL061439.
Wang, X.-F., and D. Yakir (2000), Using stable isotopes of water in evapotranspiration studies, *Hydrol. Processes*, *14*(8), 1407–1421.
Wershaw, R., I. Friedman, and S. Heller (1966), Hydrogen isotope fractionation in water passing through trees, in *Advances in Organic Geochemistry*, edited by F. Hobson and M. Speers, pp. 55–67, Pergamon, New York.
Williams, A. P., et al. (2013), Temperature as a potent driver of regional forest drought stress and tree mortality, *Nat. Clim. Change*, *3*(3), 292–297.
Williams, D., et al. (2004), Evapotranspiration components determined by stable isotope, sap flow and eddy covariance techniques, *Agric. For. Meteorol.*, *125*(3), 241–258.
Wong, S. C., I. R. Cowan, and G. D. Farquhar (1978), Leaf conductance in relation to assimilation in eucalyptus Pauciflora Sieb. ex Spreng: Influence of irradiance and partial pressure of carbon dioxide, *Plant Physiol.*, *62*(4), 670–674.
Worden, J., D. Noone, K. Bowman, and T. team (2007), Importance of rain evaporation and continental convection in the tropical water cycle, *Nature*, *445*(7127), 528–532.
Xiao, Z., S. Liang, J. Wang, P. Chen, X. Yin, L. Zhang, and J. Song (2014), Use of general regression neural networks for generating the GLASS leaf area index product from time-series MODIS surface reflectance, *IEEE Trans. Geosci. Remote Sens.*, *52*(1), 209–223.
Yakir, D., and L. Sternberg (2000), The use of stable isotopes to study ecosystem gas exchange, *Oecologia*, *123*(3), 297–311.
Yakir, D., and X.-F. Wang (1996), Fluxes of CO_2 and water between terrestrial vegetation and the atmosphere estimated from isotope measurements, *Nature*, *380*(6574), 515–517.
Yepez, E. A., D. G. Williams, R. L. Scott, and G. Lin (2003), Partitioning overstory and understory evapotranspiration in a semiarid savanna woodland from the isotopic composition of water vapor, *Agric. For. Meteorol.*, *119*(1), 53–68.
Zhou, S., B. Yu, Y. Huang, and G. Wang (2014), The effect of vapor pressure deficit on water use efficiency at the subdaily time scale, *Geophys. Res. Lett.*, *41*, 5005–5013, doi:10.1002/2014GL060741.
Zhou, S., B. Yu, Y. Zhang, Y. Huang, and G. Wang (2016), Partitioning evapotranspiration based on the concept of underlying water use efficiency, *Water Resour. Res.*, *52*, 1160–1175, doi:10.1002/2015WR017766.
Zimmermann, U., K. Münnich, W. Roether, W. Kreutz, K. Schubach, and O. Siegel (1966), Tracers determine movement of soil moisture and evapotranspiration, *Science*, *152*(3720), 346–347.

Erratum

In the originally published version of this article, there was an error in equation (1). "$T/ET_{optimal} = \frac{ET_{flux}}{min_{GPP}\ \|ET\|}$" should be "$T/ET_{optimal} = \frac{min_{GPP}\ \|ET\|}{ET_{flux}}$". The error has since been corrected in the full-text version, and this version may be considered the authoritative version of record.